J|A|C|S
ARTICLES
Published on Web 09/10/2002

Synthetic Models for the Cysteinate-Ligated Non-Heme Iron Enzyme Superoxide Reductase: Observation and Structural Characterization by XAS of an Fe^{III}−OOH Intermediate

Jason Shearer,[†] Robert C. Scarrow,[‡] and Julie A. Kovacs*,[†]

Contribution from the Department of Chemistry, University of Washington, Box 351700, Seattle, Washington 98195-1700, and Department of Chemistry, Haverford College, Haverford, Pennsylvania 19041-1392

Received December 18, 2001

Abstract: Superoxide reductases (SORs) belong to a new class of metalloenzymes that degrade superoxide by reducing it to hydrogen peroxide. These enzymes contain a catalytic iron site that cycles between the Fe^{II} and Fe^{III} states during catalysis. A key step in the reduction of superoxide has been suggested to involve HO_2 binding to Fe^{II}, followed by innersphere electron transfer to afford an Fe^{III}−OO(H) intermediate. In this paper, the mechanism of the superoxide-induced oxidation of a synthetic ferrous SOR model ($[Fe^{II}(S^{Me2}N_4(tren))]^+$ (**1**)) to afford $[Fe^{III}(S^{Me2}N_4(tren)(solv))]^{2+}$ (**2**-solv) is reported. The XANES spectrum shows that **1** remains five-coordinate in methanolic solution. Upon reaction of **1** with KO_2 in MeOH at −90 °C, an intermediate (**3**) is formed, which is characterized by a LMCT band centered at 452(2780) nm, and a low-spin state ($S = 1/2$), based on its axial EPR spectrum ($g_\perp = 2.14$; $g_\parallel = 1.97$). Hydrogen peroxide is detected in this reaction, using both ^{1}H NMR spectroscopy and a catalase assay. Intermediate **3** is photolabile, so, in lieu of a Raman spectrum, IR was used to obtain vibrational data for **3**. At low temperatures, a ν_{O-O} Fermi doublet is observed in the IR at 788(2) and 781(2) cm^{-1}, which collapses into a single peak at 784 cm^{-1} upon the addition of D_2O. This vibrational peak diminishes in intensity over time and essentially disappears after 140 s. When **3** is generated using an ^{18}O-labeled isotopic mixture of $K^{18}O_2/K^{16}O_2$ (23.28%), the vibration centered at 784 cm^{-1} shifts to 753 cm^{-1}. This new vibrational peak is close to that predicted (740 cm^{-1}) for a diatomic ^{18}O−^{18}O stretch. In addition, a ν_{O-O} vibrational peak assigned to free hydrogen peroxide is also observed ($\nu_{O-O} = 854$ cm^{-1}) throughout the course of the reaction between Fe^{II}−**1** and superoxide and is strongest after 100 s. XAS studies indicate that **3** possesses one sulfur scatterer at 2.33(2) Å and four nitrogen scatterers at 2.01(1) Å. Addition of two Fe−O shells, each containing one oxygen, one at 1.86(3) Å and one at 2.78(3) Å, improved the EXAFS fits, suggesting that **3** is an end-on peroxo or hydroperoxo complex, $[Fe^{III}(S^{Me2}N_4(tren))(OO(H))]^+$. Upon warming above −50 °C, **3** is converted to **2**-MeOH. In methanol and methanol:THF (THF = tetrahydrofuran) solvent mixtures, **2**-MeOH is characterized by a LMCT band at $\lambda_{max} = 511(1765)$ nm, an intermediate spin-state ($S = 3/2$), and, on the basis of EXAFS, a relatively short Fe−O bond (assigned to a coordinated methanol or methoxide) at 1.94-(10) Å. Kinetic measurements in 9:1 THF:MeOH at 25 °C indicate that **3** is formed near the diffusion limit upon addition of HO_2 to **1** and converts to **2**-MeOH at a rate of 65(1) s^{-1}, which is consistent with kinetic studies involving superoxide oxidation of the SOR iron site.

Superoxide reductases (SORs) are metalloenzymes that belong to a newly emerging class of enzymes, which contain a non-heme, cysteinate-ligated iron center.[1] This class of metalloenzymes performs at least two distinct functions and also includes the enzyme nitrile hydratase.[2] SORs are used as a cellular defense mechanism against oxidative stress, destroying superoxide before it can cause extensive cellular damage. Unlike superoxide dismutases, which disproportionate superoxide to afford both hydrogen peroxide and dioxygen, SORs reduce superoxide to afford only hydrogen peroxide.[3] This is especially advantageous for anaerobic organisms, which do not have the cellular machinery to deal with dioxygen. All SORs reported to date (including the enzymes rubredoxin oxidoreductase (Rbo, also known as desulfoferrodoxin) and neelaredoxin) contain, in their reduced state, a redox-active Fe^{2+} ion ligated by four equatorial histidines and a cysteinate trans to an open site.[4] As

* Corresponding author. E-mail address: kovacs@chem.washington.edu.
[†] University of Washington.
[‡] Haverford College.

(1) Kurtz, D. M., Jr.; Coulter, E. D. *Chemtracts* **2001**, *14*, 407−435.
(2) (a) Shearer, J.; Kovacs. J. A. Nitrile Hydratase: An Unusual Fe^{III} Cysteine-Ligated Metalloenzyme. *Encyclopedia of Catalysis*; John Wiley & Sons: New York, in press. (b) Kobyashi, M. *Nat. Biotechnol.* **1998**, *16*, 733−736.
(3) (a) Jovanoviæ, T.; Ascenso, C.; Hazlett, K. R. O.; Sikkink, R.; Kerbs, C.; Litwiller, R.; Benson, L. M.; Moura, I.; Moura, J. J. G.; Radolf, J. D.; Huynh, B. H.; Naylor, S.; Rusnak, F. *J. Biol. Chem.* **2000**, *275*, 28439−28448. (b) Jenney, F. E., Jr.; Verhagen, M. F. J. M.; Cui, X.; Adams, M. W. W. *Science* **1999**, *286*, 306−309.
(4) (a) Coelho, A. V.; Matias, P.; Fülöp, V.; Thompson, A.; Gonzalez, A.; Coronado, M. A. *J. Biol. Inorg. Chem.* **1997**, *2*, 680−689. (b) Andrew, P. Y.; Hu, Y.; Jenney, F. E.; Adams, M. W. W.; Rees, D. C. *Biochemistry* **2000**, *39*, 2499−2508.

Scheme 1

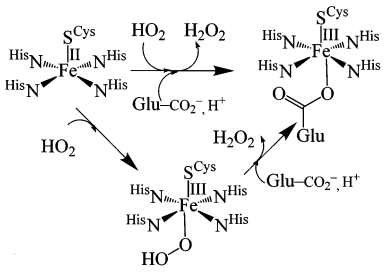

such, they resemble the heme iron enzyme cytochrome P450.[5] The hydroperoxyl radical (HO_2) oxidizes the Fe^{2+} of SOR to afford Fe^{3+} and hydrogen peroxide. Upon release of hydrogen peroxide, a glutamate coordinates to the iron center, to afford a six-coordinate ferric species (the oxidized resting state).[4b]

Recently, a number of flash photolysis studies aimed at elucidating the mechanism of SOR catalysis were reported.[6] These studies show that upon exposure of reduced SOR to HO_2 an intermediate species forms, near the diffusion limit, which has been proposed to be an $Fe^{III}-OO(H)$ species.[1] This is supported by its transient nature and electronic absorption spectrum, which contains an intense low-energy charge-transfer band characteristic of an Fe^{3+} complex.[6] This intermediate peroxide species rapidly converts to the oxidized resting state via the displacement of hydrogen peroxide by Glu47 (Scheme 1). It has been suggested that proton transfer in this final step of the mechanism involves a catalytically essential conserved Lys48.[38] A recent study demonstrated that by mutating Glu47 to alanine, the transient intermediate is stabilized, making it possible to characterize by resonance Raman. Under these conditions, an ν_{O-O} stretch is observed at 850 cm^{-1} which was attributed to a deprotonated side-on ferric peroxide species.[7] Que and Girerd have shown that a side-on ferric peroxide ($Fe^{III}(\eta^2\text{-}O_2)$) will convert to an end-on ferric hydroperoxide ($Fe^{III}(\eta^1\text{-}OOH)$) upon protonation.[8] This observation, along with the proposed involvement of a proton-transfer step in SOR catalysis, suggests that an end-on ferric hydroperoxide may be involved in the mechanism of superoxide reduction by SOR.

Non-heme $Fe^{III}-$hydroperoxo species have been implicated as important intermediates in several biological systems.[9] As such, a number of synthetic non-heme alkyl− and hydroperoxo$-Fe^{III}$ model complexes have been prepared, including those reported by Que,[8a,d,10a,f] Lippard,[10b] and Girerd,[8b] in order to gain more information about these species.[8,10] The spectroscopic characterization of $Fe^{III}-$peroxo complexes[39] is extremely difficult due to their high reactivity and photolability.[9d,11] There are even fewer structurally characterized $Fe^{III}-$peroxo complexes, with the majority of those reported being iron dimers.[10b,12] For example, Lippard[12a] recently reported the X-ray absorption spectrum of a synthetic diiron complex containing a terminal hydroperoxo, and Que and co-workers[12b] reported the crystal structure of a (μ-1,2-peroxo)diiron complex.

In a previous paper we communicated preliminary results involving the oxidation of the five-coordinate ferrous complex, $[Fe^{II}(S^{Me2}N_4(tren))]^+$ (**1**), by KO_2 in MeCN to afford the six-coordinate ferric complex $[Fe^{III}(S^{Me2}N_4(tren))(MeCN)]^{2+}$ (**2**-MeCN).[13] Hydrogen peroxide was shown to form in this reaction using a catalase assay. We now describe the mechanism of HO_2 oxidation of **1** and the observation and characterization of an $Fe^{III}-OO(H)$ intermediate.

Experimental Section

General Methods. All reactions were carried out under an atmosphere of dinitrogen or argon using a glovebox or standard Schlenk techniques. Chemical reagents purchased from commercial vendors were of the highest purity available and used without further purification. $^{18}O_2$ (23.28% isotopic enrichment) was purchased from ICON isotopes. All solvents, with the exception of tetrahydrofuran (THF) and "superdry" MeOH, were rigorously degassed and purified according to standard procedures.[14] THF was purified by refluxing it over sodium/benzophenone ketal and distilling it onto KO_2. This was then vacuum transferred immediately prior to use. Superdry MeOH was distilled from Na onto Mg/I_2, where it was refluxed for several hours and was then distilled onto 4 Å molecular sieves immediately prior to use. "Wet-MeCN" refers to MeCN that was not dried or distilled prior to use but which was rigorously degassed. D_2O was incorporated into acetone by adding 1 drop of D_2O to acetone (previously dried over 4 Å molecular sieves), followed by repeated drying and D_2O additions. IR spectra were recorded on a Perkin-Elmer 1720 FTIR either as KBr pellets or in a Beckman solution IR cell equipped with KBr windows. Electronic absorption spectra were recorded using a Hewlett-Packard 8453 diode array spectrometer. Low-temperature electronic absorption spectra were

(5) Loew, G. H.; Harris, D. L. *Chem. Rev.* **2000**, *100*, 407−420.
(6) (a) Coulter, E. D.; Emerson, J. P.; Kurtz, D. M., Jr.; Cabelli, D. E. *J. Am. Chem. Soc.* **2000**, *122*, 11555−11556. (b) Lombard, M.; Houee-Levin, C.; Touati, D.; Fontecave, M.; Niviere, V. *Biochemistry* **2001**, *40*, 5032−5040. (c) Niviere, V.; Lombard, M.; Fontecave, M.; Houee-Levin, C. *FEBS Lett.* **2001**, *497*, 171−173.
(7) Mathe, C.; Mattioli, T. A.; Horner, O.; Lombard, M.; Latour, J.-M.; Fontecave, M.; Niviere, V. *J. Am. Chem. Soc.* **2002**, *124*, 4966−4967.
(8) (a) Ho, R. Y. N.; Roelfes, G.; Hermant, R.; Hage, R.; Feringa, B. L.; Que, L., Jr. *Chem. Commun.* **1999**, 2161−2162. (b) Simaan, A. J.; Banse, F.; Mialane, P.; Boussac, A.; Un, S.; Kargar-Grisel, T.; Bouchoux, G.; Girerd, J.-J. *Eur. J. Inorg. Chem.* **1999**, 993−996. (c) Simaan, A. J.; Dopner, S.; Banse, F.; Bourcier, S.; Bouchoux, G.; Boussac, A.; Hildebrandt, P.; Girerd, J.-J. *Eur. J. Inorg. Chem* **2000**, 1627−1633. (d) Ho, R. Y. N.; Roelfes, G.; Feringa, B. L.; Que, L., Jr. *J. Am. Chem. Soc.* **1999**, *121*, 264−265.
(9) (a) Que, L., Jr.; Watanabe, Y. *Science* **2001**, *292*, 651−653. (b) Girerd, J.-J.; B., F.; Simaan, A. J. *Struct. Bonding* **2000**, *97*, 145−177. (c) Newcomb, M.; Toy, P. H. *Acc. Chem. Res.* **2000**, *33*, 449−455. (d) Solomon, E. I.; Brunold, T. C.; Davis, M. I.; Kemsley, J. N.; Lee, S.-K.; Lehnert, N.; Neese, F.; Skulan, A. J.; Yang, Y.-S.; Zhou, J. *Chem. Rev.* **2000**, *100*, 235−349. (e) Mialane, P.; Nivorojkine, A.; Pratviel, G.; Azéma, L.; Slany, M.; Godde, F.; Simaan, A.; Banse, F.; Kargar-Grisel, T.; Bouchoux, G.; Sainton, J.; Horner, O.; Guilhem, J.; Tchertanova, L.; Meunier, B.; Girerd, J.-J. *Inorg. Chem.* **1999**, *38*, 1085−1092. (f) Que, L., Jr.; Ho, R. Y. N. *Chem. Rev.* **1996**, *96*, 2607−2624.
(10) (a) Kim, J.; Larka, E.; Wilkinson, E. C.; Que, L., Jr. *Angew. Chem., Int. Ed. Engl.* **1995**, *34*, 2048−2051. (b) Kim K.; Lippard S. J. *J. Am. Chem. Soc.* **1996**, *118*, 4914−4915. (c) Rabion, A.; Chen, S.; Wang, J.; Buchanan, R. M.; Series, J.-L.; Fish, R. H. *J. Am. Chem. Soc.* **1995**, *117*, 12356−12357. (d) Roelfs, G.; Lubben, M.; Chen, K.; Ho, R. Y. N.; Meetsma, A.; Genseberger, S.; Hermant, R. M.; Hage, R.; Mandal, S. K.; Young, V. G.; Zang, Y.; Kooijman, H.; Spek, A. L.; Que, L., Jr.; Feringa, B. L. *Inorg. Chem.* **1999**, *38*, 1929−1936. (e) Wada, A.; Ogo, S.; Watanabe, Y.; Mukai, M.; Kitagawa, T.; Jitsukawa, K.; Masuda, H.; Einaga, H. *Inorg. Chem.* **1999**, *38*, 3592−3593. (f) Zang, Y.; Kim, J.; Dong, Y.; Wilkinson, E. C.; Appelman, E. H.; Que, L., Jr. *J. Am. Chem. Soc.* **1997**, *119*, 4197−4205. (g) Bernal, I.; Jensen, I. M.; Jensen, K. B.; McKenzie, C. J.; Toftlund, H.; Tuchagues, J.-P. *J. Chem. Soc., Dalton Trans.* **1995**, 3667−3669. (h) Simaan, A. J.; Banse, F.; Mialane, P.; Kargar-Grisel, T.; Bouchoux, G.; Boussac, A.; Un, S.; Girerd J.-J. *Eur. J. Inorg. Chem.* **1999**, 993−996.
(11) Lehnert, N.; Ho, R. Y. N.; Que, L., Jr.; Solomon E. I. *J. Am. Chem. Soc.* **2001** *123*, 8271−8290.
(12) (a) Mizoguchi, T. J.; Kuzelka, J.; Spingler, B.; DuBois, J. L.; Davydov, R. M.; Hedman, B.; Hodgson, K. O. Lippard, S. J. *Inorg. Chem.* **2001**, *40*, 4662−4673. (b) Dong, Y.; Yan, S.; Young, V. G., Jr.; Que, L., Jr. *Angew. Chem., Int. Ed. Engl.* **1996**, *35*, 618−620. (c) Ookubo, T.; Sugimoto, H.; Nagayama, T.; Masuda, H.; Sato, T.; Tanaka, K.; Maeda, Y.; Okawa, H.; Hayashi, Y.; Uehara, A.; Suzuki, M. *J. Am. Chem. Soc.* **1996**, *118*, 701−702. (d.) Friant, P.; Goulon, J.; Fischer, J.; Ricard, L.; Schappacher, M.; Weiss, R.; Momenteau, M. *Nouv. J. Chim.* **1985**, *9*, 33−40. (e) Kitajima, N.; Tamura, N.; Amagai, H.; Fukui, H.; Moro-oka, Y.; Mizutani, Y.; Kitagawa, T.; Mathur, R.; Heerwegh, K.; Reed, C. A.; Randall, C. R.; Que, L., Jr.; Tatsumi, K. *J. Am. Chem. Soc.* **1994**, *116*, 9071−9085.
(13) Shearer, J.; Nehring, J.; Kaminsky, W.; Kovacs, J. A. *Inorg. Chem.* **2001**, *40*, 5483−5484.
(14) Perrin, D. D.; Armarego, W. L. F.; Perrin, D. R. *Purification of Laboratory Chemicals*, 2nd ed.; Pergamon Press: Elmsford, NY, 1980.

recorded in a custom-built low-temperature copper-block sample holder inserted into a stainless steel cryostat and cooled to −90 °C by a stream of cold nitrogen gas. EPR spectra were recorded on a Bruker EPX CW-EPR spectrometer operating at X-band frequency at 130 K. Solution-state magnetic moments were calculated using the Evans' method, corrected for superconducting solenoids, on a Bruker DPX 300 FTNMR spectrometer.[15] The temperature of all NMR experiments was calculated using van Geet's method.[16] Solid-state magnetic measurements were recorded on a Quantum Design MPMS-5S SQUID magnetometer.

Preparation of [$Fe^{II}(S^{Me2}N_4$(tren))](PF_6) (1). 3-Mercapto-3-methyl-2-butanone (236 mg, 2.00 mmol) and tris(2-aminothyl)amine (267 mg, 2.00 mmol) were dissolved in a methanolic solution (25 mL) of NaOH (80 mg, 2.00 mmol) and cooled to −30 °C. To this, a solution of $FeCl_2$ (258 mg, 2.00 mmol) in MeOH (10 mL) was added dropwise, followed by the addition of 2.00 mmol of $NaPF_6$ (334 mg). This reaction mixture was stirred overnight at room temperature and then filtered through a bed of Celite. The volatiles were removed from the filtrate, and the resulting brown solid was dissolved in MeCN, filtered through a bed of Celite, and then concentrated to ∼5 mL. Diethyl ether (25 mL) was layered over top of this solution, and the two layers were allowed to diffuse together. After 2 days, a pale-green powder formed which was highly sensitive to trace amounts of oxygen (476 mg, 61%).[17] Electronic absorption (MeCN; λ_{max} (ϵ)): 262 (4 700), 357 (sh), 410 (sh) nm. IR (KBr pellet): $\nu_{C=N}$ 1593 cm^{-1}.

Preparation of [$Fe^{III}(S^{Me2}N_4$(tren))(MeCN)](BPh_4)$_2$·MeCN (2-MeCN). 3-Mercapto-3-methyl-2-butanone (574 mg, 4.00 mmol) and tris(2-aminothyl)amine (534 mg, 4.00 mmol) were dissolved in a methanolic solution (25 mL) of NaOH (164 mg, 4.00 mmol) and cooled to −30 °C. $FeCl_3$ (650 mg, 4.00 mmol) was dissolved in 20 mL of methanol, cooled to −30 °C, and added dropwise to the cold ligand solution while stirring. A deep purple solution formed instantly. Sodium tetraphenylborate (1.37 g, 4.00 mmol) was then added in 15 mL of MeCN, and the solution changed to a deep blue. The solution was filtered, the volatiles were removed by vacuum, and the resulting dark blue powder was dissolved in a minimal amount of MeCN. The undissolved salts were then removed by filtration through a bed of Celite followed by addition of diethyl ether. After 24 h blue crystals of [$Fe^{III}(S^{Me2}N_4$(tren))(MeCN)](BPh_4)$_2$·MeCN had formed (237 mg, 23% yield). Dissolution of these crystals in MeOH afforded the purple methanol-bound complex [$Fe^{III}(S^{Me2}N_4$(tren))(MeOH)]$^{2+}$ (**2**-MeOH), which appears to be indefinitely stable as a solution but is not isolable as a solid. Electronic absorption (MeCN; λ_{max} (ϵ)): 296 (sh), 467 (800), 582 (1975) nm. Electronic absorption (MeOH; λ_{max} (ϵ)): 290 (4120), 511 (1765) nm. EPR (MeCN/toluene glass, 130 K): $g_\perp = 2.12$, $g_\parallel = 1.98$. IR (KBr pellet): $\nu_{C\equiv N}$ 2243 cm^{-1}, $\nu_{C=N}$: 1615 cm^{-1}. Magnetic moment (300 K, solid state): $\mu_{eff} = 2.00\mu_B$. Magnetic moment (304 K solution state, MeCN): $\mu_{eff} = 2.12\mu_B$. Magnetic moment (301 K solution state, MeOH): $\mu_{eff} = 3.92\mu_B$. Anal. Calcd. for $FeC_{61}H_{68}N_5SB_2$: C, 74.54; H, 6.88; N, 7.24. Found: C, 74.43; H, 6.84; N, 7.86.

Generation of [$Fe^{III}(S^{Me2}N_4$(tren))(OOH)](PF_6) (3). A methanolic solution of **1** was cooled to −90 °C in a methanol/liquid nitrogen bath. A THF solution (also cooled to −90 °C) containing a 1.1-fold excess of potassium superoxide (solubilized with 18-crown-6) was then injected into the methanol solution of **1**. This instantly produced an intense orange solution, which slowly converted to a purple solution (with the same electronic spectrum as **2**-MeOH) within 10 min at −90 °C (Figure S-1 of the Supporting Information). When it is generated in this manner, **2**-MeOH decomposes into an insoluble brown material and 3-methyl-2-butanone-3-disulfide at ambient temperature (Figures S-3 and S-4 of the Supporting Information). The orange intermediate is stable for at least 2 weeks as a frozen solution at 77 K. Low-temperature electronic absorption spectrum (−90 °C, MeOH/THF; λ_{max} (ϵ)): 301 (sh), 323 (9760), 452 (2780) nm. IR: ν_{O-OH} 788, 781 cm^{-1}; ν_{O-OD} 784 cm^{-1}; $\nu^{18}{}_{O-}{}^{18}{}_{OH}$ 753 cm^{-1}. EPR (MeOH/THF glass (5:2), 130 K): $g_\perp = 2.14$, $g_\parallel = 1.97$ (Figure S-2 of the Supporting Information).

XAS Sample Preparation and Data Collection. Complex **1** (25 mg) was dissolved in 250 μL of MeOH:THF (5:2), injected into an aluminum sample holder between two pieces of 0.001 in. yellow translucent electrical tape (3M, catalog no. 1205, Minneapolis, MN) and quickly frozen in liquid nitrogen. Complex **3** was generated by injecting a THF solution of [18-crown-6(K)]O_2 into a solution of **1** in methanol at −90 °C. This solution was then injected into a cold aluminum sample holder (∼−20 °C) between two pieces of electrical tape and quickly frozen in liquid nitrogen. The purple methanol-bound product (**2**-MeOH) generated by superoxide oxidation was prepared in a manner similar to **3**, except the solution was allowed to warm to room temperature prior to its injection into the sample holder. Data were collected at the National Synchrotron Light Source (Brookhaven National Laboratories, Upton, NY) on beamline X-18B in fluorescence mode using a 13-element Ge solid-state fluorescence detector (Canberra). A helium Displex cryostat was used to maintain the samples at a constant 77 K throughout the data collection. A Si(111) double-crystal monochromator was detuned 50% for harmonic rejection. X-ray energies were calibrated by simultaneous measurement of the absorption spectrum of a piece of Fe foil (first inflection point assigned to 7111.2 eV).[18a] The spectra were measured in 5 eV increments in the preedge region (6960−7100 eV), 0.5 eV increments in the edge region (7100−7126 eV), 1.5 eV increments just above the edge (7126−7171 eV), and 3 eV increments in the EXAFS region (7171−7910 eV).

XAS Data Analysis. The fluorescence-detected XAS was corrected for detector dead time and self-absorption, and the baseline and edge shapes were established with preliminary refinements using the procedures we have described previously.[36a] All XAS analysis and plotting were performed using in-house designed macros for the

(15) (a) Evans, D. A. *J. Chem. Soc.* **1959**, 2003−2005. (b) Live, D. H.; Chan, S. I. *Anal. Chem.* **1970**, *42*, 791−792.
(16) Van Geet, A. L. *Anal. Chem.* **1968**, *40*, 2227−2229.
(17) This compound proved extremely air-sensitive and would not give a consistent elemental analysis even from ground crystals examined from the same batch.

(18) (a) Bearden, J. A.; Burr, A. F. *Rev. Mod. Phys.* **1967**, *39*, 78−124. (b) Scott, R. A. *Methods Enzymol.* **1985**, *117*, 414−459. (c) Ankudinov, A. L.; Rehr, J. *J. Phys. Rev.* **1997**, *B56*, R1712−R1715.
(19) Scarrow, R. C.; Stickler, B. S.; Ellison, J. J.; Shoner, S. C.; Kovacs, J. A.; Cummings, J. C.; Nelson, M. J. *J. Am. Chem. Soc.* **1998**, *120*, 9237−9245.
(20) Bunker, G.; Hasnain, S.; Sayers, D. In *X-ray Absorption Fine Structure*; Hasnain, S. S., Ed.; Ellis Horwood: New York, 1991; pp 751−770.
(21) Sawyer, D. T.; Valentine, J. S. *Acc. Chem. Res.* **1981**, *14*, 393−400.
(22) Mahapatra, S.; Halfen, J. A.; Tolman, W. B. *J. Am. Chem. Soc.* **1996**, *118*, 11575−11586.
(23) Shearer, J.; Kaminsky, W.; Kovacs, J. A. Manuscript in preparation.
(24) Schwartz, D. A.; Shearer, J.; Kovacs, J. A.; Gamelin, D. Unpublished results.
(25) (a) Ahmad, S.; McCallum, J. D.; Shiemke, A. K.; Appelman, E. H.; Loehr, T. M.; Sanders-Loehr, J. *Inorg. Chem.* **1988**, *27*, 2230−2233. (b) McCandlish, E.; Miksztal, A. R.; Nappa, M.; Sprenger, A. Q.; Valentine, J. S.; Stong, J. D.; Spiro, T. G. *J. Am. Chem. Soc.* **1980**, *102*, 4268−71.
(26) Solomon, E. I.; Lever, A. B. P. *Inorganic Electronic Structure and Spectroscopy*; Wiley-Interscience: New York, 1999; Vol. 1, p 365.
(27) (a) Dong, Y.; Ménage, S.; Brennan, B. A.; Elgren, T. E.; Jang, H. G.; Pearce, L. L.; Que, L., Jr. *J. Am. Chem. Soc.* **1993**, *115*, 1851−1859. (b) Broadwater, J. A.; T, J.; Loehr, T. M.; Loehr, J.-S.; Fox, B. G. *Biochemistry* **1998**, *37*, 14664−14671.
(28) Harris, D. L.; Loew, G. H. *J. Am. Chem. Soc.* **1998**, *120*, 8941−8948.
(29) Drago, R. S. *Physical Methods for Chemists*, 2nd ed.; Saunders College Publishing: Ft. Worth, TX, 1992; p 156.
(30) Warning: in one of four attempts, this reaction caused an explosion powerful enough to disintegrate the reaction flask. Rosenthal, I. *J. Labeled Compd. Radiopharm.* **1976**, *12*, 317−318.
(31) Roe, A. L.; Schneider, D. J.; Mayer, R. J.; Pyrz, J. W.; Widom, J.; Que, L., Jr. *J. Am. Chem. Soc.* **1984**, *106*, 1676−1681.
(32) Randall, C. R.; Shu, L.; Chiou, Y.-M.; Kagen, K. S.; Ito, M.; Kitajima, N.; Lachicotte, R. J.; Zang, Y.; Que, L., Jr. *Inorg. Chem.* **1995**, *34*, 1036−1039.
(33) Zhang, Y.; Pavlosky, M. A.; Brown, C. A.; Westre, T. E.; Hedman, B.; Hodgson, K. O.; Solomon, E. I. *J. Am. Chem. Soc.* **1992**, *114*, 9189−9191.
(34) Padden, K. M.; Krebs, J. F.; Trafford, K. T.; Yap, G. P. A.; Rheingold, A. H.; Borovik, A. S.; Scarrow, R. C. *Chem. Mater.* **2001**, *13*, 4305−4313.
(35) (a) Brown, I. D.; Altermatt, D. *Acta Crystallogr., Sect. B* **1985,** *41*, 244−247. (b) Thorp, H. H. *Inorg. Chem.* **1998**, *37*, 5690−5692. (c) Garner, C. D. *Physica B* **1995**, *209*, 714−716.
(36) Scarrow, R. C.; Brennan, B. A.; Cummings, J. G.; Jin, H.; Duong, D. J.; Kindt, J. T.; Nelson, M. J. *Biochemistry* **1996**, *35*, 10078−10088.

computer program *Igor Pro* 3.15 (Wavemetrics: Lake Oswego, OR). The nomenclature used to describe the EXAFS region is in accord with common usage.[18b] FEFF 7.02[18c] was used to generate amplitude (f) and phase functions (α) for the Fe−N, Fe−S, Fe−O, and Fe−C scattering, and E_0 for the simulations was set to 7124.5 eV, as previously described.[19] Bond lengths and disorder factors for **1, 2**-MeOH, and **3** were first refined using unfiltered k^2-weighted data from $k = 2.2-14.3$ Å^{-1}, and then the refinements were repeated using Fourier filtered data (FT, 2.2−14.3 Å^{-1}; BT, 0.8−3.2 Å); the results of both types of fits were practically identical since the differences in refined parameters were less than the estimated uncertainties in the parameters. To use the error estimation technique recommended by the International Workshop on Standards and Criteria in EXAFS (see below), we report the results from the Fourier filtered fits.

The reported error index used in evaluating the likelihood of the different models (lower value means more likely) is ϵ^2, defined as

$$\epsilon^2 = [n_{idp}/(n_{idp} - n_p)]R^2 \quad (1)$$

where n_{idp} is the number of data points in the $k^2(\chi)$, n_p is the number of refined parameters, and R^2 is the minimized residual between 2.2 and 14.0 Å^{-1}:

$$R^2 = \mathrm{av}[(y_{data} - y_{calc})/\sigma_{data}]^2 \quad (2)$$

In eq 2, y_{data} is the experimental (Fourier-filtered) $k^2(\chi)$, y_{calc} is the calculated (Fourier-filtered) $k^2(\chi)$, σ_{data} is the noise in the XAS spectrum (set to 0.05 Å^2 for unfiltered spectra based on previous work[19] and to 0.03 Å^{-2} for the Fourier filtered $k^2(\chi)$ spectra based on the root-mean-square magnitude of the back-transform between $r' = 3.6$ and 6.0 Å of the data for **3**). For the Fourier-filtered fits, $n_{idp} = 18.5 = \pi^{-1}\Delta r'\Delta k$ (where Δk and $\Delta r'$ refer to the ranges used in the Fourier filtering). Using criteria established by the International Workshops on Standards and Criteria in EXAFS,[20] any model that gives shell-specific ϵ_s^2 values within one of the minimum achieved value should be considered a model consistent with the EXAFS data, although models with lower ϵ_s^2 values may be considered more likely.

The baseline and edge simulations of the XAS included a "default" model for the EXAFS of four nitrogen atoms bonded at one distance and the sulfur atom bonded at a second (longer) distance. The refined baseline and edge height was then held constant for subsequent fits of the EXAFS region only. Two additional shells containing a refined number of carbon scatterers at ~3.0 and 3.5 Å were then added to the EXAFS model. An additional oxygen shell containing one oxygen-scatterer was then placed in either or both of the first- and second-coordination spheres to see how this affected the errors in the refined fits. Only in cases when ϵ^2 decreased by at least 1 were these additional shells deemed to be present.

Bond valence sums analysis (BVS)[35] of the EXAFS data was then performed according to eq 3:

$$\mathrm{BVS} = \Sigma s_{ij} \quad (3)$$

where s_{ij} is the valance of individual bonds described by

$$s_{ij} = \exp[(R_o - R_{ij})/0.37] \quad (4)$$

where R_o is the bond-length of a valence unit and R_{ij} is the experimentally determined bond length.[35a] The values used for R_o were 1.76 Å for Fe−O, 1.83 Å for Fe−N, and 2.15 Å for Fe−S.[36]

Kinetic Measurements. A 0.100(1) mM THF/MeOH (9:1) solution of **1** and a 20.0(1) mM THF:MeOH (9:1) solution of KO_2 (as the 18-crown-6 salt) were injected together into a stopped-flow instrument equipped with an OLIS−USA rapid-scanning monochromator and an OLIS−USA detector. The complete formation of **3** occurred within the first 3 ms of the reaction and was therefore not observed. However, the conversion of **3** to **2**-MeOH was observed. The kinetic trace for the conversion of **3** to **2**-MeOH (Figure S-5 of the Supporting Information) was then fit to a first-order rate law.

Results and Discussion

It was previously reported that the addition of solid KO_2 to a "wet" MeCN solution of the reduced iron complex $[Fe^{II}(S^{Me2}N_4(tren))]^+$ (**1**) rapidly produced the oxidized six-coordinate ferric complex $[Fe^{III}(S^{Me2}N_4(tren))(MeCN)]^{2+}$ (**2**-MeCN).[13] Solutions of oxidized **2**-MeCN are blue and characterized by a LMCT band in the electronic absorption spectrum centered at 582(1975) nm,[13] which compares well with that previously reported for the blue oxidized form of superoxide reductase (SOR) recorded at pH = 9.2 (λ_{max} = 610(~1900) nm).[6] The superoxide-induced oxidation of **1** required that the solvent contain trace amounts of water, presumably in order to facilitate protonation of superoxide[21] or metal-bound peroxide. If rigorously dried MeCN or THF is used, the conversion of **1** to **2**-solv (solv = MeCN or THF) is not observed, even at low temperatures (vide infra). Instead, a brown polymeric substance, which cannot be readily identified, rapidly forms. This could be the result of ligand decomposition caused by O_2^--attack at either one of the coordinated amine N−H bonds or the thiolate sulfur. Another possibility is that high-valent metal−oxo-induced oxidative N-dealkylation occurs under these "dryer" conditions. Oxidative N-dealkylation reactions have been shown by Tolman and co-workers to occur following the decomposition of Cu−oxo species.[22] This would require that O−O bond cleavage occurs to afford a high-valent Fe−oxo derivative of **2**. However, added olefins are not oxidized in this reaction, and H-atom abstraction from weak C−H (9,10-dihydroanthrocene) or O−H (TEMPO−H) bonds does not occur, suggesting that oxidative damage does not proceed via a high-valent Fe−oxo species.

Since the MeCN used in this experiment contained trace amounts of water (which could lead to the disproportionation of superoxide), and since the solubility of KO_2 in MeCN is low, it was difficult to establish the stoichiometry of the reaction which affords **2**-MeCN via the direct addition of solid KO_2 to **1**. Instead, 18-crown-6 was dissolved in THF followed by the addition of KO_2. This THF solution was then injected into a MeCN solution of **1**. In this manner, the amount of KO_2 added could be quantified on the basis of the amount of 18-crown-6 utilized. It was determined that a slight excess of KO_2 is needed (1.1:1.0) in order to observe complete conversion of **1** to **2**-MeCN. This indicates that the stoichiometry for the oxidation reaction is 1:1, with a small sacrificial amount of KO_2 disproportionating to dioxygen and hydrogen peroxide due to the presence of water.

Hydrogen peroxide is detected in the reaction between **1** and HO_2 using a catalase assay. Catalase disproportionates hydrogen peroxide to water and O_2(g). If an aqueous solution of catalase is added to the reaction mixture containing **1** and HO_2, immediate rapid bubbling of O_2 is observed. In contrast, immediate bubbling does not occur when catalase is added to solutions containing only HO_2 and no metal complex, even when the solvent is wet. A similar control showed that bubbling does not occur when HO_2 is absent and only the metal complex is present. Hydrogen peroxide is also detected in the reaction between **1** and HO_2 by ^{1}H NMR spectroscopy. A peak grows in at 9.43 ppm (H_2O_2) in the ^{1}H NMR spectrum within 30 s following the addition of HO_2 to **1**. After 60 s, this ^{1}H NMR

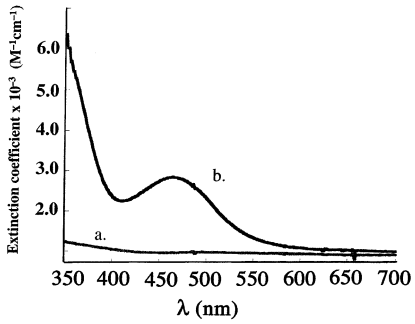

Figure 1. Electronic absorption spectrum of $[Fe^{II}(S^{Me2}N_4(tren)]^+$ (a) vs $[Fe^{II}(S^{Me2}N_4(tren))]^+$ (**1**) + 1.1 equiv (18-crown-6-K^+)O_2^- in MeOH/THF (1:9) at −90 °C to afford hydroperoxo intermediate $[Fe^{III}(S^{Me2}N_4(tren))(OOH)]^+$ (**3**) (b).

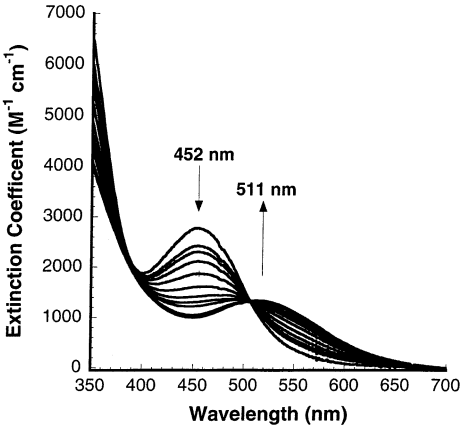

Figure 2. Electronic absorption spectrum showing that $[Fe^{III}(S^{Me2}N_4(tren))(OOH)]^+$ (**3**; λ_{max} = 452 nm (2780 M^{-1} cm^{-1})), generated by adding 1.1 equiv of (18-crown-6-K^+)O_2^- to $[Fe^{II}(S^{Me2}N_4(tren))]^+$ (**1**) at −90 °C in MeOH/THF, cleanly converts to $[Fe^{III}(S^{Me2}N_4(tren))(MeOH)]^{2+}$ (**2**-MeOH; λ_{max} = 511 nm (1765 M^{-1} cm^{-1}) nm) over the course of ∼10 min at −90 °C.

Scheme 2

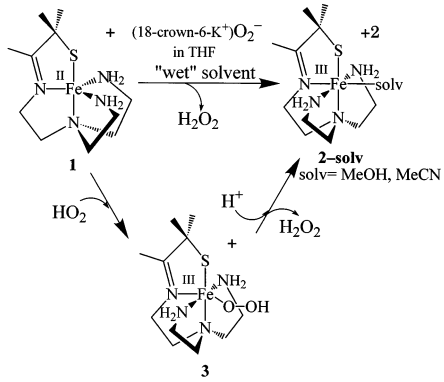

peak diminishes substantially, and after 90 s, this peak completely disappears.

When **2**-MeCN is generated via HO_2-induced oxidation of **1**, it decomposes within about 2 min. This is presumably due to oxidative ligand damage induced by H_2O_2 attack at the thiolate sulfur. The loss of the H_2O_2 signal in the ^1H NMR experiment directly correlates with the increase in the metal-containing decomposition product, which suggests that H_2O_2 is responsible for the decomposition of **2**-MeCN. An analysis of the decomposition products by ^1H NMR (Figure S-2 of the Supporting Information) and mass spectrometry (Figure S-3 of the Supporting Information) showed 3-methyl-2-butanone-3-disulfide to be the major isolable product (see Supporting Information). The remainder of the reaction mixture contained an insoluble polymeric material that possibly incorporates the oxygen atoms from hydrogen peroxide. Identical decomposition products are obtained if a 30% solution of H_2O_2(aq) is added directly to **2**-MeCN.

Observation of $[Fe^{III}(S^{Me2}N_4(tren))(OOH)]^+$ (3). Addition of potassium superoxide to a wet MeCN solution of **1** immediately affords **2**-MeCN upon mixing.[13] No intermediates are observed in this reaction, even if the temperature is lowered to the freezing point of MeCN (−41 °C). When **1** is dissolved in MeOH at ambient temperature, addition of a THF solution of KO_2 (solubilized with 18-crown-6) immediately affords $[Fe^{III}(S^{Me2}N_4(tren))(MeOH)]^{2+}$ (**2**-MeOH) upon mixing. This complex is characterized by a LMCT band centered at 511 nm (1765 M^{-1} cm^{-1}) and an intermediate spin state (S = 3/2). Methanol-bound **2**-MeOH also forms when $[Fe^{III}(S^{Me2}N_4(tren))(MeCN)]^{2+}$ (**2**-MeCN) is dissolved in MeOH.

As shown in Figure 1, at temperatures near the freezing point of MeOH (−90 °C) *an intermediate is observed* in the reaction between HO_2 and **1**. At this temperature, one sees the featureless electronic absorption spectrum of **1** (Figure 1a) convert to one that has a LMCT band centered at 452 nm (2780 M^{-1} cm^{-1}; Figure 1b). This contrasts dramatically with the spectral changes observed in the ambient temperature experiment, where the spectrum of **1** converts to one that has an LMCT band centered at 511 nm (1765 M^{-1} cm^{-1}). Even at −90 °C, the species which initially forms (λ_{max} = 452 nm) is unstable and cleanly converts to **2**-MeOH ((λ_{max} = 511 nm) after about 10 min (Figure 2). This indicates that the species which initially forms (λ_{max}= 452 nm) is a *transient intermediate*. The position of the LMCT band (Figure 1b) suggests that this transient intermediate is an oxidized Fe^{III} species, possibly an Fe^{III} peroxo or hydroperoxo complex ($[Fe^{III}(S^{Me2}N_4(tren))(OOH)]^+$ (**3**); Scheme 2). The blue shift of this band, relative to solvent-ligated **2**-MeCN (582 nm) or **2**-MeOH (511 nm), would be consistent with an increase in electron density at the metal, due to the coordination of an anion (e.g., HO_2^-) or a change in the nature of the ligand orbitals (e.g., sulfur → peroxo) involved in the charge-transfer transition.

When intermediate **3** is generated in MeOH/THF (1:9) in an EPR tube, an axial signal is observed ($g_\perp$ = 2.14, $g_\parallel$ = 1.97; Figure S-1 of the Supporting Information) at 130 K, indicating that the iron is in the +3 oxidation state and low spin. The g-spread of this signal is similar to that of other low-spin ferric complexes in this ligand environment.[13,23] A low-spin state and narrow g-spread are also consistent with what has been observed with other Fe^{III}−peroxo species.[9a,10] Upon warming the EPR sample of **3** to room temperature and then re-recording the spectrum at 130 K, the signal corresponding to this low-spin Fe^{III} species is lost. This is also consistent with the assignment of **3** as a transient intermediate and consistent with the formation of **2**-MeOH, which is S = 3/2 and therefore not observable at 130 K, as the end-product in the reaction of **1** with HO_2 in MeOH.

Vibrational Spectrum of $[Fe^{III}(S^{Me2}N_4(tren))(OOH)]^+$ (3). Since it seemed likely that the intermediate produced in the reaction of **1** with HO_2 was a metastable Fe^{III}−peroxo species, we attempted to identify Fe−O or O−O stretches in the resonance Raman spectrum. Unfortunately, **3** proved to be extremely photolabile, decomposing even if an off-resonance wavelength was selected, at short exposure times, with laser

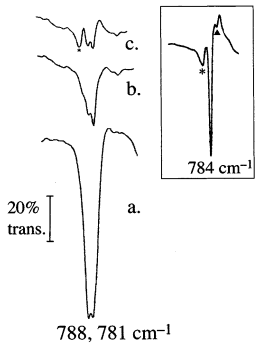

Figure 3. Infrared spectrum of the hydroperoxide intermediate $[Fe^{III}(S^{Me2}N_4(tren))(OOH)]^+$ (**3**) formed in the reaction between $[Fe^{II}(S^{Me2}N_4(tren))]^+$ (**1**) and 1.1 equiv of (18-crown-6-K^+)O_2^- in wet acetone/THF at −70 °C after ∼20 s (a), as it begins to warm after ∼40 s (b), and as it warms further after ∼100 s (c). Insert depicts the IR spectrum which results upon the addition of D_2O in place of H_2O. * = vibration associated with the ligand; ▲ = residual protio Fe^{III}−OOH.

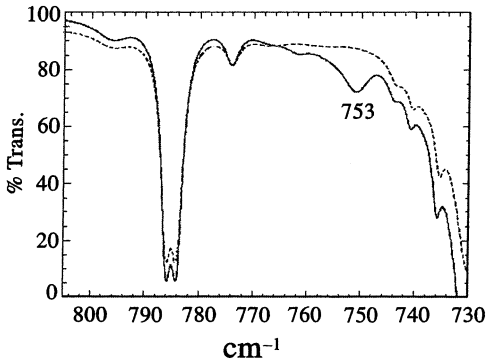

Figure 4. Infrared spectrum of the hydroperoxide intermediate formed in the reaction between $[Fe^{II}(S^{Me2}N_4(tren))]^+$ (**1**) and a 23.28% $^{18}O_2^-/^{16}O_2^-$ mixture (—) vs 100% $^{16}O_2^-$ (--) in wet acetone at −70 °C.

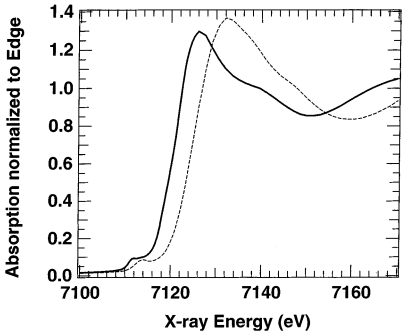

Figure 5. XANES region of the XAS for **1** (solid line) vs **3** (dashed line).

power less than 10 mW. This photolability is also consistent with the behavior of several other derivatives of **2**-L (where L = MeCN, azide, and cyanide).[24] Vibrational data for intermediate **3** could, on the other hand, be obtained by FT-IR. IR samples of **3** were generated by injecting an acetone solution of **1** (as the chloride salt, cooled near its freezing point −95 °C) into a cold (−95 °C) acetone solution of KO_2 (as the 18-crown-6 salt). The resulting solution was then quickly injected into a precooled solution IR cell, and the spectrum recorded. The progress of the reaction was then monitored over 2 min (Figure 3). In the first 20−40 s, a species with stretching frequencies at 788 and 781 cm^{-1} is observed. This is where one would expect to see the ν_{O-O} of a metal−peroxide.[8a,b,10d,25] The symmetrical splitting of this vibrational peak is most likely due to Fermi resonance,[26] which involves the coupling between two vibrations of similar energies. Fermi coupling has been observed with other Fe^{III}−peroxo species as well.[27] Addition of D_2O causes the Fermi doublet shown in Figure 3 to collapse into a single, sharper peak at 784 cm^{-1} (see inset of Figure 3). This is what one would expect if Fermi coupling were responsible for the observed doublet in the protio spectrum.[29] The absence of a shift in frequency upon deuteration is predicted[39] and has been observed with other synthetic Fe^{III}−OOH systems.[8d] When $K^{18}O_2$ (solubilized with 18-crown-6), made via the addition of $^{18}O_2$ (23.28% isotopic enrichment) to the K salt of benzhydrol (CAUTION),[30] is used in place of $K^{16}O_2$, a new stretch appears in the vibrational spectrum at 753 cm^{-1} (Figure 4). The observed isotopic shift of 31 cm^{-1} is close to that predicted (44 cm^{-1}) for a diatomic oxygen species.

Although the ν_{O-O} stretch observed for **3** is lower in energy than usual for an Fe^{III}−peroxo species (typical range: 806−900 cm^{-1}), this is not without precedent.[8a,d,39] Que and coworkers, for example, recently described an Fe^{III}−OOH hydroperoxo complex that has an ν_{O-O} stretch at 790 cm^{-1}.[8a] The low frequency of this stretch was attributed to the fact that the peroxo species was protonated and coordinated to a low-spin Fe^{III} center.[10d] This was further supported by recent normal coordinate analysis and DFT calculations[39] on Que's non-heme Fe^{III}−OOH complex,[8d] and calculations performed on the heme center of cytochrome P450 by Harris and Loew,[28] who noted that single protonation of the distal oxygen of a ferric−peroxide species causes significant weakening of the O−O bond. It was also speculated that the addition of a second proton to the proximal oxygen would lead to the release of hydrogen peroxide, resulting in the formation of oxidized Fe^{III}.[28] This is similar to what is described herein; i.e., Fe^{II}−**1** is oxidized to Fe^{III}−**2** by superoxide, in wet solvents, forming H_2O_2 in the process.

As shown in Figure 3, the ν_{O-O} vibrational peak observed in the reaction between Fe^{II}−**1** and superoxide diminishes in intensity and essentially disappears after 140 s. In addition, an ν_{O-O} vibrational peak, assigned to free hydrogen peroxide in acetone, is also observed ((ν_{O-O} = 854 cm^{-1}) throughout the course of the reaction and is strongest after 100 s (Figure S-5 of the Supporting Information). Since it seemed likely from the vibrational data that an Fe^{III}−OOH species forms as an intermediate in the reaction between Fe^{II}−**1** and superoxide, we sought to further characterize this intermediate using X-ray absorption spectroscopy.

X-ray Absorption Spectroscopy of 1, 2-MeOH, and 3. X-ray absorption spectroscopy (XAS) experiments were performed in order to gain more detailed structural information about the intermediate species, **3**, formed in the reaction outlined in Scheme 2. Complex **3** was generated by injecting a cold (−90 °C) THF solution of 18-crown-6 solubilized potassium superoxide into a cold (−90 °C) MeOH solution of **1**, loading the sample into a prechilled holder (ca. 30 s) and quickly freezing the samples in liquid nitrogen. A standard of **1** was prepared in a similar manner except potassium superoxide was not added. XAS measurements were then performed at 77 K on frozen solutions of **1** and **3**.

The XANES region of the XAS for **1** vs **3** shows a number of differences between the two complexes (Figure 5). First, the edge transition occurs at a higher energy for **3** relative to **1**, which indicates a change in oxidation state from Fe^{II} (**1**) to Fe^{III} (**3**).[8a,b,25] This finding supports the conclusions reached from

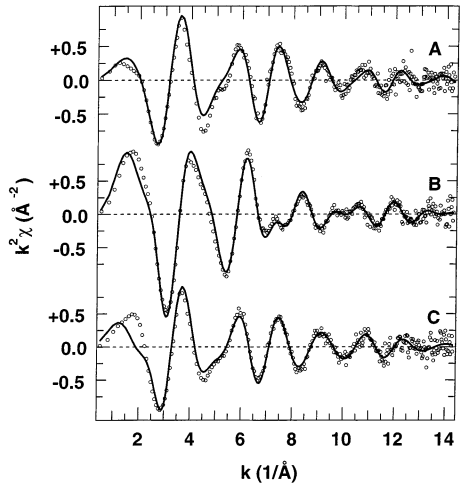

Figure 6. Plot of the EXAFS region ($k^2(\chi)$) and best fits for $[Fe^{II}(S^{Me2}N_4(tren))]^+$ (**1**, a), $[Fe^{III}(S^{Me2}N_4(tren))(OOH)]^+$ (**3**, b), and $[Fe^{III}(S^{Me2}N_4(tren))(MeOH)]^+$ (**2**-MeOH, c). The circles depict the experimental data, and the solid line is the best fit of the spectra.

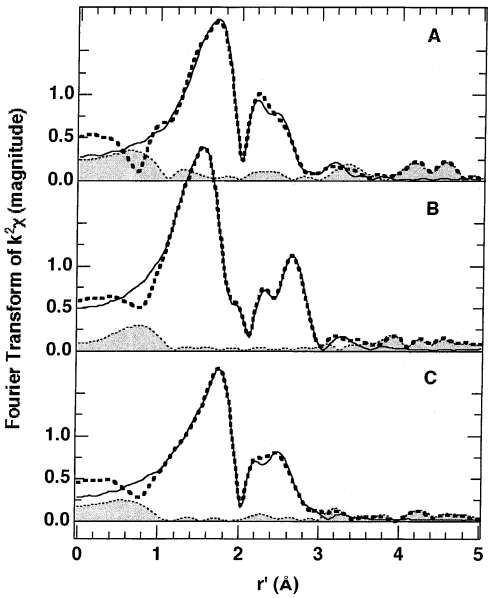

Figure 7. Plot of the EXAFS FT magnitude ($k^2(\chi)$ transformed between k = 2.2 and 14.3 Å^{-1}) and best fits for $[Fe^{II}(S^{Me2}N_4(tren))]^+$ (**1**, a) $[Fe^{III}(S^{Me2}N_4(tren))(OOH)]^+$ (**3**, b), and $[Fe^{III}(S^{Me2}N_4(tren))(MeOH)]^+$ (**2**-MeOH, c). The dashed lines depict the experimental data, the solid line is the best fit of the spectra, and the shaded region indicates the magnitude of the FT difference spectrum.

the analysis of both the electronic absorption and EPR spectra of **3**. The small peak found just before the edge, which results from the symmetry disallowed 1s → 3d transition, is of similar height and area in the two complexes; the area obtained by our procedure is 19 eV % in both cases (the % is relative to the edge height; see Table S-1 of the Supporting Information). It has been previously shown by Que and co-workers that the intensity of the 1s → 3d transition is directly related to the symmetry (coordination number) of a complex, with the peak area/height being larger for a less centrosymmetric complex (i.e. a five-coordinate complex) vs a higher symmetry complex (i.e. a six-coordinate or four-coordinate square-planar complex).[31,32] The area determined for the preedge peak of **3** lies exactly halfway between those obtained by the same procedure for the 1s → 3d peak for the five-coordinate Fe^{III} nitrile hydratase model $[Fe^{III}(S_2{}^{Me2}N_3(Pr,Pr))]^+$ (26 eV %) and its six-coordinate azide derivative $[Fe^{III}(S_2{}^{Me2}N_3(Pr,Pr))(N_3)]$[19] (12 eV %); indicating that **3** most likely contains a highly asymmetric distribution of bond lengths around a six-coordinate iron. Since the area of this transition is typically smaller for an Fe^{II} complex vs an Fe^{III} complex in a similar ligand environment,[33] the 19 eV % area, along with lower energy (relative to that in **3**) of this peak in **1**, suggest that, in solution, **1** is five-coordinate Fe^{II}. Analysis of the EXAFS region of **1** and **3** is consistent with these findings.

The unfiltered (UF) and Fourier transformed (FT) EXAFS regions of the XAS of **1**, **2**-MeOH, and **3** are displayed in Figures 6 and 7, and the results of various refinements are collected in the Supporting Information. The results from the best fits are also shown in Table 1. The EXAFS region of **1** refined well for a complex containing four nitrogen scatterers and one sulfur scatterer at distances of 2.19(2) and 2.33(2) Å from the metal center, respectively (Table 1). These distances agree well with the crystallographic parameters for both **1**[13] and reduced SOR.[4b] In addition to these two shells, refinements for **1** improved when two Fe−C shells of about four carbon atoms each were included in the model at 3.00(4) and 3.54(7) Å. The structure of **1** suggests that there should be eight carbon atoms at ca. 3.0 Å, but, in complexes with five-membered chelate rings, we have found through multiple-scattering simulations employing FEFF 7.02 that the scattering amplitude can be reduced considerably due to destructive interference from multiple-scattering EXAFS.[34] The apparent presence of a longer (3.5 Å) Fe−C shell is presumed to be due primarily to multiple scattering involving the methyl groups of the ligand.

In fitting the EXAFS data for **1**, **3**, and **2**-MeOH, we added a sixth oxygen ligand to the EXAFS fitting model to determine whether EXAFS can detect a solvent methanol or peroxide ligand bound to iron in solution. In the case of **1,** the extra scatterer led to a *slight* increase in the error determined for the fits ($\epsilon^2 = 2.6$ for six-coordinate **1** vs 2.5 for five-coordinate **1**), which does not entirely rule out the possible coordination of a solvent ligand. However, the six-coordinate model included an unreasonably large σ^2 for the 4 N shell (0.026 Å^2) and a negative σ^2 for the 1 O shell (−0.001 Å^2), and for these reasons was discounted.

The five coordinate geometry for **1** (which is consistent with the crystal structure) is consistent with bond valence sum analysis (BVS). BVS has been previously utilized to verify that the data obtained from EXAFS refinements are consistent with the spin state of the metal complex.[35,36] As originally proposed,[35a] BVS analysis requires a calculation using a different set of r_0 values (the nominal single bond length for a M−X bond) for each possible oxidation and spin state of the metal. This is done so that the BVS will equal the oxidation state when the oxidation/spin state is correctly assigned. But, as we have previously noted,[36] the requirement that BVS = oxidation state is arbitrary (not supported by modern theories of chemical bonding), so we prefer to discard this requirement and use the same values of r_0 for all possible oxidation/spin states (we use values originally designed for high-spin Fe^{III}). For a metal ion in a given oxidation and spin state, the BVS is usually found to be within ±0.2 of the average value found for known crystal structures (for Fe^{III} these numbers are $S = 1/2$, BVS ∼ 4.10 and $S = 5/2$, BVS ∼ 3.00, and for Fe^{II} these numbers are $S = 2$, BVS ∼ 2.30 and $S = 0$, BVS ∼ 4.20).[36] Within a given

Table 1. Results from Fits to Fourier Filtered $k^2(\chi)$ Spectra[a]

	FeN shell ($n = 4$)		FeS shell ($n = 1$)		FeO shells ($n = 1$)			FeC shells			
	R (Å)	σ^2 (Å^2)	R (Å)	σ^2 (Å^2)	R (Å)	σ^2 (Å^2)	n	R (Å)	σ^2 (Å^2)	ϵ^2	BVS
1	2.19(2)	0.011(6)	2.33(2)	0.003(3)			4(2)	3.00(4)	0.007(10)	2.5	2.13
							3(3)	3.54(7)	0.00(1)		
3	2.01(1)	0.005(2)	2.33(2)	0.010(4)	1.86(3)	0.002(7)	11(4)	3.05(2)	0.009(4)	3.0	3.85
					2.78(3)	0.001(3)	19(9)	3.44(2)	0.02(1)		
2-MeOH	2.19(4)	0.008(13)	2.31(7)	0.005(8)	1.94(10)	0.01(2)	2(5)	3.01(8)	0.005(18)	1.1	2.79
							8(12)	3.5(1)	0.02(4)		

[a] Only fits with the lowest ϵ^2 and nonnegative σ^2 are shown; fits using other coordination models are shown in Tables S-2 though S-4 of the Supporting Information.

oxidation state, as the number of ligands is increased about the metal center, the average bond lengths will also increase (indicating a decrease in the valency of any one bond), yet the BVS in the complex remains the same. Using the EXAFS derived bond lengths from the five-coordinate model, we obtain a BVS = 2.13 for **1**, which is within the range expected for $S = 2$ Fe^{II}. Thus the BVS analysis is consistent with the conclusion from the XANES analysis that the iron center in **1** remains five-coordinate in MeOH/THF at 77(1) K.

In contrast to **1**, the EXAFS region of **3** refined best for a six-coordinate complex containing one oxygen scatterer (at 1.86(3) Å; Table 1), four nitrogen scatterers (at 2.01(1) Å), and one sulfur scatterer (at 2.33(2) Å). Because of their very similar scattering abilities and distances, the nitrogen and oxygen shells could be combined into a single shell of five atoms (modeled as four nitrogen atoms and one oxygen atom at 1.99(1) Å) with only a slight decrease in the quality of the fits ($\epsilon^2 = 3.2$ vs 3.0). In addition to the innersphere oxygen scatterer, a second oxygen scatterer at a distance of 2.79(6) Å from the metal center was found to significantly improve the fits (the best fit without this scatterer (Table S-3 of the Supporting Information) has $\epsilon^2 = 4.6$). This Fe−O distance is too long to be a covalent bond, indicating that this oxygen is located in the secondary coordination sphere. Density functional theory (DFT) calculations using the B3LYP/LCAVP* level of theory[37] indicate that ∼2.8 Å is where one would expect to find the uncoordinated oxygen of an end-on hydroperoxo ligand coordinated to Fe^{III}, if the coordinated oxygen were at a distance of ∼1.9 Å (the distance observed by EXAFS).

The oxidation state and bond length changes on going from **1** to **3** will lead to changes in second-sphere distances and bond angles, and these changes can explain the increased amplitude of the Fe−C scattering shells modeled with $r = 3.05$ and 3.44 Å. Replacement of either of these shells by an Fe−Fe scattering shell at 2.8−3.2 Å led to an increase in the error of the calculated fits for **3**, indicating that if the complex is an Fe−O−O−Fe dimer, the bridge is sufficiently flexible to allow a large range of Fe−Fe distances. Furthermore, the observed stretching frequency of the O−O bond is ∼100 cm^{-1} lower than that which is typically observed for peroxide-bridged Fe−O−O−Fe dimers.[10−12,39] Also, the BVS (BVS = 3.85) and EPR spectrum (Figure S-1 of the Supporting Information) of **3** indicate that **3** is $S = 1/2$, suggesting that it is most likely not an antiferromagnetically coupled Fe^{III} dimer. On the basis of these observations, we conclude that **3** is most likely not a μ-peroxo-bridged species.

The 1s → 3d transition observed in the preedge region of the X-ray absorption spectrum of **2**-MeOH is not as high and less distinct than that of **3**, which is consistent with a six-coordinate ferric complex. Analysis of the EXAFS region of **2**-MeOH (Figure 6 and Table 1) solved best for a six-coordinate iron complex with four nitrogen scatterers (2.19(4) Å), one oxygen scatterer (1.94(10) Å), and one sulfur scatterer (2.31(7) Å). As was observed with **3**, refinements of the data for **2**-MeOH suffered when an iron scatterer was included in the refinement parameters. The Fe−O distance of **2**-MeOH is rather short, suggesting that perhaps the methanol is deprotonated. However, addition of base (slightly less than 1 equiv) to reactions in which **2**-MeOH is generated via the dissolution of **2**-MeCN in MeOH, results in rapid decomposition. All attempts at preparing an alkoxide derivative of **2** resulted in the formation of intractable solids.

Rate of Oxidation of 1. Vibrational and X-ray absorption data indicate that **3** is most likely an Fe^{III} complex with an end-on hydroperoxo ligand. To determine the rate at which this intermediate forms, and is then converted to **2**-MeOH, this reaction was monitored by stopped-flow kinetics at ambient temperature. Complex **1** was dissolved in a THF:MeOH mixture (9:1) and injected into a freshly prepared solution of 18-crown-6 solubilized potassium superoxide in THF:MeOH (9:1), to afford **3** within the first 3 ms of the reaction. Thus, rates for the formation of **3** could not be determined using stopped-flow techniques. Complex **3** converts to solvent-ligated **2**-MeOH at a rate of 65(1) s^{-1}. These observations are in agreement with flash photolysis studies on the SOR enzyme, which have shown that the intermediate observed during SOR catalysis is formed near the diffusion limit and converts to the glutamate-ligated form of the enzyme at a rate of 40 s^{-1}.[6] Thus, on the basis of the spectroscopic studies and kinetic data reported herein, we propose that oxidation of **1** by HO_2 proceeds via an Fe^{III}−hydroperoxo intermediate **3**. Protonation of the hydroperoxo ligand by a nearby solvent molecule then promotes the displacement of hydrogen peroxide from **3**, to afford **2**-solv (Scheme 2).

Conclusions

In the model compound described herein, the thiolate sulfur is cis, as opposed to trans, to the open-binding site, as it is in the SOR enzyme. Despite this deviation in structure, the similarities in the chemistry taking place in both the enzyme and our model compound is striking. Both systems display superoxide reductase activity showing no signs of dismutase

(37) Calculated using the computer package *Titan* (Wave function: Irvine, CA). Discussed in: Shearer, J. Models For Metalloenzymes Containing Sulfur-Metal Bonds. Doctoral Thesis, University of Washington, Seattle, WA, 2001.
(38) Adams, M. W. W.; Jenney, F. E., Jr.; Clay, M. D.; Johnson, M. K. *J. Biol. Inorg. Chem.* **2002**, *7*, 647−652.
(39) Lehnert, N.; Neese, F.; Ho, R. Y. N.; Que, L., Jr.; Solomon, E. I. *J. Am. Chem. Soc.* **2002**, *124*, in press.

activity. The model compound $[Fe^{II}(S^{Me2}N_4(tren))]^+$ (**1**) catalyzes this reaction via the innersphere reduction of HO_2, to afford a metastable Fe^{III}−hydroperoxo intermediate. It is likely that the enzyme operates in a similar fashion. Furthermore, the rates of hydrogen peroxide displacement via the coordination of a sixth ligand are comparable for both the enzyme and the synthetic model. This is despite the fact that there is not a trans labilizing thiolate sulfur in the model system.[2a]

Acknowledgment. The NIH is gratefully acknowledged for their support of this work (Grant No. GM 45881). The authors thank Daniel Gamelin and Ed Solomon for helpful discussion, Dana Schwartz for doing resonance Raman experiments, and Jim Mayer for use of his stopped-flow instrumentation (UW/NIH Grant GM50422). J.S. was provided a predoctoral fellowship through the EPA (Grant No. 91594801-0). Research carried out (in part) at the National Synchrotron Light Source, Brookhaven National Laboratory was supported by the U.S. Department of Energy, Division of Materials Sciences and Division of Chemical Sciences. The EPR spectrometer was provided courtesy of the Center for Ecogenetics and Environmental Health, UW Center (Grant No. P30 ES07033) from the National Institute of Environmental Health Sciences, NIH.

Supporting Information Available: Tables of EXAFS refinement results for **1**, **3**, and **2**-MeOH, an EPR spectrum of **3**, kinetic traces for the conversion of **1** to **2**-MeOH, the ^{1}H NMR and high-resolution mass spectra of the decomposition products formed in the reaction between **1** + O_2^- at ambient temperature, and vibrational data for **3** after 140 s (PDF). This material is available free of charge via the Internet at http://pubs.acs.org.

JA012722B